SAND 96-l 172
Unlimited Release
Printed May 1996

Distribution
Category UC- 126

ANALYSIS OF STRATEGIC PETROLEUM RESERVE BUBBLE POINT PRESSURE DATA

S. E. Lott
Underground Storage Technology Department
Sandia National Laboratories
Albuquerque, NM 87 185

ABSTRACT

Mathematical models are presented to predict the bubble point pressure for 48 1 cavern oil samples withdrawn from the Bryan Mound, West Hackberry, Big Hill, and Bayou Choctaw Strategic Petroleum Reserve sites. The predicted bubble point pressure is compared to experimentally measured bubble point pressure to resolve potential sources of error introduced to the experimental analysis. In order to gain a higher level of confidence in the measurement of the bubble point pressure, a stochastic analysis of the data is recommended in the future.

EXECUTIVE SUMMARY

Between 7/25/91 and 6/4/95, 481 cavern oil samples were withdrawn from the Bryan Mound, the West Hackberry, the Big Hill, and the Bayou Choctaw Strategic Petroleum Reserve sites and were analyzed in the laboratory for composition and bubble point pressure. These pressurized bomb samples are the least expensive method of determining the gas content of oil stored in the Strategic Petroleum Reserve because they are being gathered for other sampling purposes. The data were characterized by high bubble point pressures, unusually high nitrogen concentrations, and overall inconsistency. Interpretation of the data to predict the true bubble point data is an important factor in determining the rate of deliverability of Strategic Petroleum Reserve crude oil.

Mathematical models are presented to predict the bubble point pressure as a function of the sample composition. The results of these models are used to identify the sources of error in acquiring the compositional and bubble point data. Potential variables in the error analysis include cavern site, sample date, sample depth, sample composition, sampling method, and laboratory procedure.

The high nitrogen concentration is suggestive of air contamination in the sample analyzed. Measurement of the oxygen content is recommended for future samples to quantify air infiltration. The liquid flash samples are suspect; therefore, cavern composition should be calculated based solely on the vapor composition. The Big Hill samples in particular have unusually poor agreement between measured and modeled bubble point pressures.

The concentration of the lower molecular weight fractions in the flash liquid fraction is too low. This error manifests itself in lower calculated bubble point pressures. Use of the vapor phase concentrations and equilibrium constants to predict the liquid composition was found to be a reasonable approximation, and introduced less error than direct use of the liquid fraction compositional data. A stochastic technique was shown to be useful in reconciling which measured variables introduce the majority of error in determining the “true” bubble point pressure; significant error was introduced in the measurement of the gas to liquid flash ratio and the bubble point pressure. A stochastic analysis of the data is recommended in the future in order to minimize the impact of errors and gain a higher level of confidence in the measurement of the bubble point pressure.

Acknowledgments

The author would like to acknowledge Tom Hinkebein for helpful discussions during this study. Brian VanderHyden (Los Alamos National Laboratory) co-wrote a key simplifying step in deriving the equations for the stochastic analysis. The author would like to thank Tom Hinkebein and Martin Molecke for reviewing this document and for their suggestions.

Contents

List of Tables

List of Figures

I. Background

The existence of gas in the United States Strategic Petroleum Reserve (SPR) oil caverns has been observed over many years. Salt miners have encountered pockets of gas and most domal salt mines in Louisiana have been declared "gassy" by the Mine Safety and Health Administration. The gas is introduced into the stored oil in a cavern predominately by diffusion from the surrounding salt. The gas composition is primarily methane with lesser quantities of carbon dioxide and other gasses. At cavern storage pressures, typically 1000 to 2000 psig, the gas is readily absorbed into the crude oil. During oil withdrawal, oil is transferred at a reduced pressure through surface pipelines and tanks, thereby releasing some of the dissolved gas. The release of large quantities of the dissolved gas may exceed both EPA emission standards for tanks and safety limits for handling. Understanding the propensity for gas release during a cavern drawn down is critical to maintaining both a safe and an EPA-compliant operation. Additional background on gassy oil intrusion into SPR underground storage is found elsewhere'.

Gas intrusion into the stored oil and subsequent release has been recently addressed through a program of degassing the stored crude oil. Predicting the rate of gas intrusion from the surrounding salt into the crude oil, i.e., the rise of bubble point pressure (BPP) as a function of time, is essential in scheduling the frequency of crude oil degassing. In order to predict the frequency for degassing the stored crude oil, samples are removed and analyzed for composition and BPP at a known temperature. In the pressurized bomb method of obtaining this data, a pressurized crude oil sample is withdrawn from the cavern, flashed at near atmospheric pressure, the gas and liquid fractions of the product flash analyzed for composition, and the gas:liquid (G/L) ratio measured. This information is used to calculate the crude oil composition in the cavern. Therefore, the cavern composition is a quantity based on other measured values and is not of itself a measured value. In a separate analysis, the BPP of the cavern sample is measured at a known temperature.

Between 7/25/91 and 6/4/95, 481 pressurized bomb cavern samples were withdrawn and analyzed from the Bryan Mound, West Hackberry, Big Hill, and Bayou Choctaw SPR sites. Interpretation of the data was made difficult by excessively high BPPs, unusually high nitrogen concentrations, and overall inconsistent results. This document reviews the sources of the bias and errors in the raw data and makes recommendations for future cavern sample analyses. The data compiled during the flash procedure of the pressurized samples were used to predict the BPP employing five different mathematical models. The predicted BPP was compared to the experimentally measured BPP and potential causes for bias and/or error were examined. In addition, a stochastic technique was then used to distinguish relative sources of error in the experimental procedure. The results from the BPP modeling and the stochastic technique identified the key sources of experimental error. The predominate errors identified are measurement of the gas:liquid flash ratio, the BPP, and the liquid composition. Minor changes in the experimental

procedure and the analysis of the data will produce BPP values with a higher degree of confidence.

II. Bubble Point Pressure Theoretical Approach

Five mathematical models were formulated to predict the BPP for the SPR caverns. Two of the models employ cubic equations of state, while three models are based on vapor liquid equilibria (VLE) data for binary mixtures and Dalton's Law. The cubic equations of state are the Soave-Redich-Kwong (SRK) and the Peng-Robinson (PR). The three models based on VLE data predict the BPP as a function of the liquid composition, the vapor composition, or the reservoir composition.

II.A. BPP Based on Cubic Equation Of State and Mixing Rules

The method of calculating the flash composition of the liquid and vapor phases draws upon equations from various sections in a text by Reid, Prausnitz, and Poling[2]. After each converged flash calculation, the pressure is adjusted in an iterative fashion until the vapor fraction is driven to near zero. The nomenclature for the following equations is in Table 1. A separate model was written for the liquid and vapor phases. A model for each phase was written to predict the fugacity coefficient for that phase; the ratio of the fugacity coefficients is used to calculate the relative concentration of the species in each phase.

The SRK equation of state is used in the compressibility form:

$$Z^3 - Z^2 + (A-B-B^2)Z - AB = 0 \quad (1)$$

The PR equation of state is also used in the compressibility form:

$$Z^3 - (1-B)Z^2 + (A-2B-3B^2)Z - AB + B^2 + B^3 = 0 \quad (2)$$

For the liquid phase, the smallest real root of Z is used. For the vapor phase, the largest real root of Z is used. For both equations of state, the parameters A and B are defined as follows:

$$A = a_m P/R^2T^2 \quad (3)$$
$$B = b_m P/RT \quad (4)$$

The values of a, and b_m are dependent on the composition of the liquid and the vapor and are calculated from the values of a and b for the species in the phase. The mixing rules for the vapor phase for both the SRK and the PR models are the same:

$$a_m = \Sigma_i \Sigma_j y_i y_j (a_i a_j)^{1/2} (1-k_{ij}) \quad (5)$$
$$b_m = \Sigma_i y_i b_i \quad (6)$$

The interaction parameter (k_{ij}) relates non-ideal behavior between the phase species and has different values for each model. Values for the k_{ij}'s are found in the literature[3]. For the liquid phase, the y_i's would be replaced with x_i's. For each of the species, the values

of a and b need to be calculated for each of the equations of state. For the SRK equation of state, a_i is defined as:

$$a_i = 0.08664RT_c/P_c \tag{7}$$

For the PR equation of state, the leading coefficient for a_i is 0.07780. For the SRK equation of state, the value of b_i is,

$$b_i = 0.42748R^2T_c^2(1+f_w(1-T_r^{1/2}))^2/P_c \tag{8}$$
$$f_w = 0.48 - 1.574w - 0.176w^2 \tag{9}$$

and for the PR equation of state,

$$b_i = 0.45724R^2T_c^2(1+f_w(1-T_r^{1/2}))^2/P_c \tag{10}$$
$$f_w = 0.37464 - 1.54226\sim - 0.26992w^2 \tag{11}$$

In order to calculate the equilibrium ratio, K_i, the fugacity coefficient (ϕ_i) for the SRK model was calculated for each species in the liquid and vapor phases from the following:

$$\ln\phi_i = (b_i/b_m)(Z-1) - \ln(Z-B) + (A/B)(b_i/b_m - \delta_i)\ln(1+B/Z) \tag{12}$$

The following expression was used for the PR equation of state:

$$\ln\phi_i = (b_i/b_m)(Z-1) - \ln(Z-B) + (A/B)(b_i/b_m - \delta_i)\ln\{(Z+(1+\sqrt{2})B)/(Z+(1-\sqrt{2})B)\}/2\sqrt{2} \tag{13}$$

For both the PR and the SRK equations of state, b_i/b_m and δ_i are defined as,

$$b_i/b_m = (T_{ci}/P_{ci})/(\Sigma_j y_j T_{cj}/P_{cj}) \tag{14}$$
$$\delta_i = (2a_i^{1/2}/a_m)\Sigma_j x_j a_j^{1/2}(1-k_{ij}) \tag{15}$$

The equilibrium ratio for a species is calculated from the ratio of the fugacity coefficients for that species:

$$K_i = (\phi_i)_{liquid}/(\phi_i)_{vapor} \tag{16}$$

The liquid (xi) and vapor (y_i) mole fractions are related to the liquid fraction of the mixture (L/F), the overall cavern mole fractions (z_i), and the equilibrium ratio, K_i by the following:

$$x_i = z_i/(K_i + L/F(1-K_i)) \tag{17}$$
$$y_i = K_i z_i/(K_i + L/F(1-K_i)) \tag{18}$$

When the equations are satisfied, the sum of the liquid mole fractions will equal the sum of the vapor mole fractions.

$$\Sigma_i x_i = \Sigma_i y_i \quad (19)$$

To satisfy the equality in equation 19, the liquid fraction of the mixture is adjusted by the following relation suggested by King[4].

$$(L/F)_{new} = L/F - \Sigma_i\{(z_i(K_i-1))/(K_i + (1-K_i)(L/F))\} / \Sigma_i\{(z_i(K_i-1)^2)/(K_i + (1-K_i)(L/F))^2\} \quad (20)$$

Equations (1) through (20) allow for the flash calculation of a mixture for a given overall composition, temperature, and pressure. The flash calculation requires an iterative process since the compressibility of the vapor (or liquid) phase is dependent on the composition of the vapor (or liquid) phase. This composition, in turn, is calculated from the compressibility of the phase through the fugacity coefficients and the equilibrium ratio for each species.

Once the iterative flash calculation is converged for a given pressure and temperature, the pressure is adjusted to make the liquid fraction equal to one, i.e., to solve for the BPP. A modified Newton's method is used to adjust the pressure.

$$P_{new} = P + \alpha(1 - L/F)\{(P - P_{last})/(L/F - L_{last}/F)\} \quad (21)$$

where a is an approach parameter. a is set between 0 to 1 based on the degree of linearity of the function of P bases on L/F; a higher non-linearity requires a lower value of a for stability. At the updated value of pressure (P_{new}), a new flash calculation is made to determine a new value of L/P. The pressure is adjusted in an iterative fashion until the liquid fraction is equal to one.

Therefore, calculation of the BPP is solved in the following manner. The calculation is structured with an iterative solution for the flash calculation nested inside an iterative solution for the BPP.

1. Assume a BPP based on the composition of the vapor. Typical initial guess is 10 psia. Initial guess is raised or lowered based on stability of initial guess.
2. Assume a liquid fraction of 1.0 (no vapor fraction). Assume that the liquid composition is equal to the reservoir composition and that the vapor composition is only methane and/or nitrogen (depending on whether one or both species are present).
3. Solve for the compressibility factor for the equation of state of choice using the mixing rules outlined in equations 3-l 1.
4. Solve for the equilibrium ratios using equations 12-16.
5. Solve for the liquid (xi) and vapor (y_i) mole fractions (eqns. 17 & 18) and check convergence criteria (eqn. 19). If solution has not converged, the liquid fraction (L/P) is adjusted by equation 20 and the calculation continue at step 3.
6. After flash calculation has converged, adjust the assumed BPP in step 1 by equation 21 and solve the flash calculations for a new BPP guess. BPP converges when L/F is equal to one.

II.B. BPP Based on Vapor-Liquid Equilibria Data

Dalton's Law states that the sum of the partial pressures equals the total pressure ($P_{total} = \Sigma_i P_i$). At the bubble point pressure, the total pressure equals the BPP. Henry's Law states that the partial pressure (Pi) equals the liquid mole fraction (xi) multiplied by the Henry's Law constant ($P_i = H_i x_i$). At the BPP, the liquid mole fraction equals the total mole fraction ($x_i = z_i$). Therefore the BPP can be written as:

$$BPP = \Sigma_i H_i z_i \qquad (22a)$$

For the liquid and vapor species in the caverns, the Henry's Law constant has been modeled as an exponential function of temperature'. Thus at a chosen temperature, the BPP can be calculated directly based on a known cavern composition by equation 22a. A complication arises that the cavern composition is a calculated quantity and is a function of the liquid and vapor composition and the L/F ratio. If a concern arises in either the liquid or the vapor analysis, the cavern mole fractions (z_i) can be estimated from either the liquid mole fractions (xi) or the vapor mole fractions (y_i) by equations 17 and 18. Substituting either equation 17 or 18 into equation 22a and rearranging,

$$BPP = \Sigma_i y_i((L/F)P + (1-L/F)H_i) \qquad (22b)$$

$$BPP = \Sigma_i H_i x_i(H_i(1-L/F)/P + L/F) \qquad (22c)$$

Thus, the BPP can be directly calculated from the cavern, vapor, or liquid mole fractions using equations 22a, 22b, or 22c respectively.

II.C. Solution of BPP Models

A data set containing 481 cavern reports from Weatherly Laboratories was furnished by J. Roche of DOE/SPR/PMO in a flat file format. Due to the size of the data file, the data file was truncated and loaded into five different Excel spreadsheets, and then manipulated to organize the data in a repetitive set of entries for each cavern sample. A Visual Basic module was written to carryout the calculations outlined in section II.A. For the flash calculation, the iteration was carried out until the criteria in equation 19 was satisfied within a margin of 10^{-7}. The BPP iteration loop had a convergence criteria of $0.9999 < L/F < 1.0001$. For the calculations outlined in section II.B., calculations were carried out directly in an Excel spreadsheet.

III. Bubble Point Pressure Model Results

The bubble point pressure for 481 cavern samples was modeled using five different methods and compared to the experimentally determined BPP values. The five models were the SRK model, the PR model, and the three VLE models. The three VLE models used either the liquid, vapor, or the overall cavern composition. The difference between a modeled BPP and the experimentally measured BPP was correlated to the experimental conditions under which the samples were taken.

Results from the SRK, the PR, and the cavern composition VLE models were similar. Figure 1 illustrates the relationship of the results of the cavern composition VLE model versus the SRK and the PR models. Data that fall on the 45" line indicate perfect agreement between the VLE model and the SRK (or PR) model. In most cases, the variation between the two equation of state models (SRK and PR) is small. In addition, prediction of the BPP by way of the cavern composition VLE model is shown to agree at pressures less than 30 psia.

Since the two equations of state models yield nearly the same results, either the SRK or the PR model may be used to compare the modeled results to the experimentally measured BPP. The following analysis was made with the PR model. An arbitrary error was selected to distinguish the data in which the PR model BPP value and the experimental BPP value agreed well from the data in which the values did not agree well. For 20% of the data sets, the PR model values and the experimental BPP values agreed within ±4 psi. As additional examples, 10% of the data sets were within ±2.3 psi; 50% of the data were within f8.8 psi. In order to encompass a reasonable amount of the data, but not to increase the range of acceptability between the values of the PR and experimental BPP too high, an arbitrary acceptable error was set at ±4 psi. For cavern data sets within the ±4 psi limit, an indicator or "1" was assigned; if the data set was outside the ±4 psi range, an indicator of "0" was assigned. For the ±4 psi limit, a histogram of the species concentration data assigned a "1" indicator was compared to a histogram of the data assigned a "0" indicator. These results are shown in Figures 2-6 for CO_2, N_2, CH_4, C_2H_6, and nC_5H_{12}. The histograms for the C_3H_8, nC_4H_{10}, iC_4H_{10}, iC_5H_{12}, and C_6H_{14} data are not shown, but are similar to the nC_5H_{12} data.

For the lighter end volatile components (CO_2, N_2, CH_4, C_2H_6), the "1" series of histograms have on average a higher concentration than the "0" histograms. The skew in the concentration distribution disappears for the higher molecular weight species (C_3H_8 and higher). For example, a 95% confidence T-test on the nC_5H_{12} data predicts that the average concentration for the "0" distribution data is between 3.51% and 3.63%; for the "1" distribution data, the 95% confidence T-test is between 3.40% and 3.57%. Since these ranges overlap, no significant difference exists in the averages of the two distributions. On the other hand, the T-test 95% confidence limits for the average of C_2H_6 data for the "0" and the "1" distributions are 0.24%-0.25% and 0.26%-0.29% respectively. These ranges do not overlap and thus there is a significant difference

between the "0" and "1" distributions. In summary, for the data in which the experimental BPP did not compare favorably with the model BPP, the concentration of the light end components was, on average, lower.

For most of the cavern samples, two different sample cylinder sizes were used, 500cc and 1000cc. The data for all of the caverns were separated into two groups based on sample cylinder size. These two groups were analyzed to determine the extent that the experimental and model data were within a ±4 psi agreement. As stated above, 20% of the total data set fell within the ±4 psi range. When the two sample cylinder size groups were analyzed, 20% of each group also fell within the ±4 psi range. Therefore, no major effect of sample size seemed to impact the BPP results.

Figure 7 shows the number of samples and the agreement between the modeled and experimentally measured BPP values versus sample date on a quarterly basis. None of the experimental and modeled BPPs agreed within ±4 psi for samples taken prior to 1/93 and after 4/95. Between 1/93 and 4/95, the agreement between the BPPs increased and then decreased. The number of samples being evaluated does not correlate with the rise and fall of the percentage agreement of the BPPs, thus, a high volume of sample analysis can be discounted as an issue. Also the impact of a "learning curve" by Weatherly can be discounted since the agreement between the experimental and the modeled BPPs drops after 4/94. A partial explanation for the rise and fall in agreement may be evident in Figure 8 that shows a histogram of the sampling method versus time. There appears to be a correlation between the sampling technique and the degree of agreement between the experimentally measured and modeled BPPs. On average, the coiled tubing and skid sampling techniques yielded better agreement between the BPPs; the surface and down hole sampling techniques yielded poorer agreement (Table 2). There is an additional unascertained error since the agreement between the BPPs is less for the period from 1/95 to 6/95 than for 7/94 to 12/94, however, only the down hole sampler was used for 7/94 to 6/95. The source of this additional error would only be conjecture. Therefore, sampling techniques contributed to part of the poor agreement between the experimentally measured and modeled BPPs. Additional errors were introduced that were not attributed to a "learning curve" at Weatherly or total number of samples.

Sampling depth did not have any obvious impact on agreement between the experimental and modeled BPPs (Figure 9). The percentage of samples in which the experimentally measured BPP agreed with the modeled BPP was approximately equal to the average of 20% for all samples except for the deepest sampling. The percentage agreement between the BPPs was lower for the set of samples with a depth of 4000 to 4475 feet; however, the sample size was small with the number of samples that were within the ±4 psi bound being 2 (26 samples x 8%).

Figures 10 and 11 show the degree of agreement between the modeled and experimental BPP values by site, and the type of sampling technique used by site, respectively. The agreement between the experimental and modeled BPPs for the Bayou Choctaw, the Bryan Mound, and the West Hackberry sites are similar; for the Big Hill site, agreement

is significantly lower. Referring to Figure 11, the type and proportion of sampling methods used at Big Hill did not produce a lower correlation between the experimental and the modeled BPPs. Big Hill had the highest percentage of sampling by coiled tubing and skid (the 2 presumed best techniques) of all of the sites. Table 2 summarizes the overall agreement between the experimental and modeled BPPs by site and sample technique, and the distribution of sampling techniques by site. A "weighted average" was calculated which equals the sum of the product of the fraction of the sample type and the overall agreement of that sample type. If there was no bias between sites, then the weighted average should equal the average agreement between the experimental and modeled BPPs for the site. As shown in Table 2, the agreement between the modeled BPP and the experimental BPP for Bayou Choctaw, Bryan Mound, and West Hackberry was nearly equal to the weighted averages. The average for Big Hill (6%) is far less than the expected value based on the weighted average of 23%. To explore if the dates of sampling may have had an effect on the lower than expected Big Hill results, the sampling dates were categorized into two groups; (1) pre 1/93 and post 4/95, and (2) 4/95 through 1/95 inclusive. The results are shown in Table 3. While a higher percentage of the Big Hill samples were withdrawn during the "poorer" sampling times (group 1), the percentage is not high enough to account for the overall lower correlation between the experimental and modeled BPP at the Big Hill site. Factors other than schedule or sampling method accounted for the poor agreement between the experimental and modeled BPPs in the Big Hill samples.

As stated above, the model based on the VLE expressions agreed well with the models based on the SRK or the PR equations of state. In addition, the VLE model can be solved using the composition of the liquid (Equation 22c), the vapor (Equations 22b), or the overall cavern (Equation 22a). As a reminder, the cavern compositions are recombined values based on the composition of the liquid and vapor, and the L/F ratio. Therefore, any error associated with the liquid or vapor composition will be reflected in the predicted BPP based on the cavern composition. In order to discern contribution of error or bias from the liquid composition versus the vapor composition, the experimentally determined BPP was compared to the VLE model BPP based on the liquid or the vapor composition.

The experimentally determined BPP was compared to the VLE model BPP based on only the liquid composition (Figure 12) or only the vapor composition (Figure 13). The 45" line in Figures 12 and 13 is a reference line and represents a perfect agreement between the modeled and experimental values. In both Figures 12 and 13, the high degree of scatter infers that a significant error was introduced to one or more variables that are common to both the VLE model calculations. The VLE model results based on the liquid composition are considerably biased lower than expected as compared to the experimentally measured values. The model results based on vapor composition (Figure 13) are nearly uniformly scattered about the 45" line inferring far less bias than in the liquid composition VLE model. When the VLE model is based on only one phase (liquid or vapor) as in Figure 12 and 13, the equilibrium constants (K_i's) are used to predict the concentrations of the other phase. The L/F ratio is then used to calculate a combined

cavern composition which in turn is used to calculate the BPP. Since the model BPP results based on the liquid composition are significantly lower than the VLE model BPP results based on the vapor composition, and the bias in the vapor model is near zero, the concentration of the light ends in the liquid are less on average than expected (since the light end fraction predominately impact the BPP).

In summary, a higher degree of error exists for the samples taken at the Big Hill site that cannot be attributed to sampling scheme, date, or sample cylinder type. To a first order, there is no significant variation among the three other major sites in terms of sampling scheme, date, or sample cylinder type. For all of the samples, there is poorer comparison between the modeled and experimental BPPs when the light ends have a lower concentration. The corollary to this last statement is that there may be a loss of light ends on some samples that lead to a poorer comparison between the modeled and experimental BPPs. Finally, the liquid composition data has a high bias towards a lower modeled BPP, i.e., there was a lower than expected concentration of light ends in the liquid fraction leading to a bias towards lower modeled BPPs.

IV. Observation of Experimental Procedures

IV.A. Summary of Experimental Procedure

IV.A.1. Sample Collection and Displacement A visit was made to Weatherly Laboratories on March 12, 1996 by T.E. Hinkebein (6113) and S.E. Lott to discuss experimental procedures used in the gassy oil analysis. A pressurized crude oil sample was withdrawn at the cavern by displacing water from a sample bomb. The sample bomb was held vertical and then part or all of the water was drained from the bottom of the bomb to separate the sample into two phases for safe transport from the site to Weatherly Labs. At the laboratory, each sample was held vertical, pressurized at the bottom (liquid end) with mercury to re-form a single phase, shaken, and a small fraction of the sample was flashed at the top of the sample bomb through water to collect a gas sample for gas chromatography analysis. The mercury pump was then disconnected.

IV.A.2. Bubble Point Measurement The sample bomb was wrapped with heating tape, connected to a mercury pump, then heated to a specified temperature. The sample was slowly pressurized in a stepwise fashion, shaking the sample at each pressure step to ensure that the temperature of the sample was uniform. The procedure was continued until the sample was a single phase. The pressure of the sample was plotted versus the volume of mercury injected yielding two distinct lines of different slope, one for the two-phase system and one for the single-phase system. The slopes of the two lines are representative of the different volume compressibility of either the two-phase or single-phase sample. The intersection of the two lines yielded the experimentally determined bubble point pressure, i.e., the pressure at which the sample changed from a two-phase to a single-phase system.

IV.A.3. Vapor:Liquid Ratio Flash Measurement and GC Analysis Lastly, the sample was flashed a second time into a separation flask and the total gas and liquid production volumes measured. Weatherly stated that a typical liquid production volume was 20 cc. A Ruska gasometer was used to measure the gas production volume. The liquid sample was used to determine the liquid composition via gas chromatography analysis. Laboratory procedures for gas chromatography analysis of the liquid and gas samples were also observed. The chromatography analysis for the gas samples had excellent baseline to baseline peak separation. The chromatography analysis for the liquid samples had good peak separation.

IV.B. Conclusion of Observations

Referring to Figure 13, some of the samples had a much higher than reasonable BPP, in excess of 60 psia. In many of the unusually high experimental BPP samples, the nitrogen concentration was also abnormally high. In some fashion, nitrogen may have been introduced to some of the samples prior to gas chromatography analysis. The generalized agreement between the experimentally measured BPPs and the modeled BPPs (Figure 13) suggests that if nitrogen (air) was added to the samples, the nitrogen was introduced prior

to, or during the first mercury pressurization, since the added nitrogen affected both the gas samples and the later experimentally evaluated BPP. This fact unfortunately means that there is not enough information to calculate the cavern composition and BPP for the actual cavern conditions. However, even with some uncertain amount of nitrogen introduction to the samples, the experimental and modeled BPPs should be equal since the added nitrogen would impact both the flash gas composition and the experimentally measured BPP. This assumption is shown to be reasonable due to the minimal bias in Figure 13. Therefore, if all other variables were measured flawlessly, there would be no error shown in Figure 13; any deviation in Figure 13 from the 45" line is a consequence of additional error(s) introduced by variable(s) other than nitrogen concentration.

When the liquid sample was collected, no visible precautions were taken to minimize loss of light ends from the liquid prior to analysis by gas chromatography. Since the cavern samples have a high liquid fraction (typically greater than 0.99 molar ratio), even a small loss of the light ends in the liquid fraction would have significant impact on the light ends cavern composition and, in turn, the calculated BPP. When the calculated BPP is based solely on the liquid composition, a high negative bias is evident compared to the experimentally measured BPP (Figure 12). In addition, Figures 2-6 showed that samples with lower light end concentrations have, on average, poorer agreement between the modeled and experimental BPPs. Considering the modeling results and the experimental observations, the accuracy of the liquid composition is questionable.

The liquid to feed ratio (L/P) or the equivalently expressed gas to liquid ratio (G/L), had a relatively high degree of associated uncertainly. The liquid fraction production volume was reported by Weatherly to be about 20 cc. The gas measurement was also reported to be ± 2 cc gas. In terms of a G/L molar ratio, this error range is ± 0.001 moles gas per mole liquid. A G/L error of ± 0.001 is significant since the G/L production ratio ranged from about 0.0025 to 0.0300.

The bubble point pressure was measured using a 2½" gauge with 1 psi increments. Thus, it is plausible that the pressure was only measured within ± 1-2 psig. In addition, the methods used to measure the BPP required extrapolation of two lines to yield the bubble point pressure. Based on observations by Weatherly, the error associated with the extrapolation was estimated to be on the order of an additional ± 1 psig.

V. Statistical Adjustment Approach

In order to reconcile the appropriate magnitude of the errors associated with the variables in the gassy oil analysis, a stochastic technique was used. The technique uses a constrained least squares approach where other balances must be satisfied. This technique uses the Lagrange Method of Multipliers'.

If the data is denoted as the variables S_i, a set of adjusted variables (S_i^*) could be chosen such that an optimization function, F, is minimized.

$$F = \Sigma_i (S_i - S_i^*)^2 / E_i \tag{23}$$

E_i is the associated variance of the variables S_i, and the summation in equation 23 is over the n variables. For a least squares regression, F would be minimized by differentiating F with respect to S_i^*, setting dF/dS_i^* to zero and solving the equations for S_i^*. However, F cannot be minimized since the S_i^* are not independent and are constrained by balances. Two balances are formed:

$$M_1 = BPP_{model} - BPP_{experiment} \tag{24}$$

$$M_2 = \Sigma_i y_i - 1 \tag{25}$$

Equation 24 states that the experimentally measured BPP and the modeled BPP must be equal. Equation 25 states that the sum of the vapor mole fraction must sum to one. Due to the introduction of the two balances, two new parameters are introduced (hi, λ_2) and the optimization function augmented:

$$L = F + \lambda_1 M_1 + \lambda_2 M_2 \quad \underline{\text{or}}$$

$$L = \Sigma_i (S_i - S_i^*)^2 / E_i + \lambda_1 M_1 + \lambda_2 M_2 \tag{26}$$

The new function, L, is differentiated with respect to S_i^*, and set to zero to minimize L:

$$\partial L / \partial S_i^* = 0 = -2(S_i - S_i^*)/E_i + \lambda_1 \varphi_{1i} + \lambda_2 \varphi_{2i} \tag{27}$$

where:

$$\varphi_{ji} = \partial M_j / \partial S_i^* \quad \text{at } S_i = S_i^* \tag{28}$$

Equation 27 is solved for $S_i - S_i^*$:

$$S_i - S_i^* = E_i(\lambda_1 \varphi_{1i} + \lambda_2 \varphi_{2i})/2 \tag{29}$$

If equation 29 is multiplied by φ_{ji} and then summed over n:

$$\Sigma_i \varphi_{ji}(S_i - S_i^*) = \Sigma_i \varphi_{ji} E_i (\lambda_1 \varphi_{1i} + \lambda_2 \varphi_{2i})/2 \tag{30}$$

A Taylor series is written for M_j at S_i and expanded about S_i^*.

$$M_j \big|_{Si} = M_j \big|_{Si*} + \Sigma_i \partial M_j / \partial S_i^* \big|_{Si*} (S_i - S_i^*) + \text{higher order terms} \tag{31}$$

The first term is simply M_j. The second term is equal to zero since the balances are satisfied at S_i^*. The derivative in the third term is re-written as φ_{ji} (per equation 28). Therefore equation 3 1 is equal to:

$$M_j = \Sigma_i \varphi_{ji}(S_i - S_i^*), \tag{32}$$

for values of S_i close to S_i^*. Substituting equation 32 into equation 30,

$$M_j = \Sigma_i \varphi_{ji} E_i (\lambda_1 \varphi_{1i} + \lambda_2 \varphi_{2i})/2 \tag{33a}$$

If equation 33 is written for 2 balances (equations 24 and 25):

$$M_1 = \Sigma_i \varphi_{1i} E_i (\lambda_1 \varphi_{1i} + \lambda_2 \varphi_{2i})/2 \tag{33b}$$

$$M_2 = \Sigma_i \varphi_{2i} E_i (\lambda_1 \varphi_{1i} + \lambda_2 \varphi_{2i})/2 \tag{33c}$$

To solve for adjusted variable values, S_i^*, the partial derivatives φ_{ji} (equation 28) must first be calculated. Equations 33b and 33c are then solved for λ_1 and λ_2. The values of S_i^* are then calculated in equation 29. An iterative calculation is required since the functions M_1 and M_2 are not linear with respect to S_i^*, therefore only an approximate calculation of the derivative φ_{ji} is possible until S_i is equal to S_i^*.

To minimize introduced error from the liquid composition data, and to simplify calculations, the VLE vapor composition BPP model was used for calculation of BPP_{model} (equation 24). Previous results (Figures 1 & 13) have shown that this is a reasonable assumption. The adjusted variables were the vapor mole fractions (y_i's), the gas to liquid flash ratio (G/L), the experimentally measured BBP, and Henry's Law constant for the C_7+ fraction. Inclusion of the last variable requires some addition clarification.

The C_7+ vapor fraction is not representative of the C_7+ liquid fraction. A typical average molecular weight of the C_7+ liquid fraction is about 210 which can be approximated by a C_{17} n-paraffin. Weatherly stated that the C_7+ fraction from analysis of the gas samples is primarily C_7, C_8, and C_9. Since the gas C_7+ fraction could be estimated to be a C_8 species on average, relating a C_8 species in the gas phase to a C_{17} species in the liquid phase is not rigorous. Unfortunately, without making additional assumptions about boiling point distributions, the raw data was not reported to properly relate the C_7+ fractions of the vapor and liquid. An assumption was made that the C_7+ fraction did not significantly contribute to the BPP. Therefore, the liquid phase C_7+ fraction was assumed to be C_8 and the Henry's Law constant was used to predict the liquid composition from the gas composition. To check if the C_7+ fraction did indeed have an impact on the BPP, the Henry's Law constant for C_7+ was allowed to be a variable with a high related variance (see below).

Inspection of equations 29 and 33 show that the calculated values of S_i^* are dependent on the variances (E_i). The variances are estimated from an understanding of the degree of

experimental uncertainty in obtain the data. For the vapor mole fractions, Weatherly used a standard boiling point column that had excellent baseline to baseline integration. A typical standard deviation (σ_i) for gas chromatography for such a circumstance is 5% of the integration area down to a base error for small peaks. Between a relative concentration of 1% to 2%, the σ_i was set at 10% of the peak error; below a relative concentration of 1%, a base error σ_i of 10% of 1% (0.001) was assumed. The σ_i for the G/L ratio and the experimental BPP were assumed to be 0.001 molar ratio and 2 psig, respectively, based on discussions with Weatherly (see page 10). Although the values for Henry's Law for C_7+ were not expected to change, relatively large σ_i values were assumed to encompass Henry's Law constants from C_6 to C_{14}. The variances were calculated from the square of the estimated standard deviations.

VI. Statistical Adjustment Results

The algorithm outlined in section V was used to statistically adjust the data to make the experimental BPP equal to the modeled BPP while requiring the data to maintain mass balance on the gas species. The variables that underwent notable adjustment, i.e., in which $S_i - S_i^*$ was significant, were the experimentally measured BPP and the G/L ratio. The nitrogen concentration underwent minor adjustment for higher nitrogen concentrations. A plot of the nitrogen composition data and the adjusted nitrogen composition data is shown in Figure 14. The other vapor concentrations were not adjusted to any significant degree. The Henry's Law constants for C_7+ were not significantly adjusted; the assumption that the C_7+ fraction did not contribute to the error in the modeled BPP was substantiated.

The adjusted BPPs are plotted versus the measured BPPs in Figure 15. The degree of scatter increases with a negative bias for greater values of BPP. The experimentally measured BPP values were, on average, measured too high for higher BPPs and too low for lower BPPs. Figure 16 shows the other major adjusted variable, the measured gas to liquid ratio from the flashing of the sample. The scatter in Figure 16 increases with greater G/L values with the bias changing from negative to positive as the BPP increased. The shape of the scatter in Figures 15 and 16 is dictated by equation 23. As the magnitude of S_i becomes larger for a constant difference between S_i and S_i^*, the value of F (optimization function) becomes larger since F is related to the square of the difference. Thus for larger values of either BPP (Figure 15) or G/L (Figure 16), the degree of adjustment is greater.

Since the G/L ratio is adjusted, the modeled BPP is changed. A plot of the adjusted modeled BPP versus the modeled BPP is shown in Figure 17. Comparing Figures 15 and 17, it is interesting that for BPP under 20 psia, the modeled BPP requires far less adjustment as compared to the experimentally measured BPP. This is a consequence of the small values of the G/L ratio for low BPPs. At low BPPs little adjustment of the G/L ratio is possible since the G/L ratio is already very low. As the G/L ratio becomes larger for higher bubble point pressures, more adjustment to the G/L ratio is possible thereby allowing an increased adjustment to the modeled BPP. For BPPs of 30 psia or greater, the scatter in the experimentally measured BPP and the modeled BPP are similar.

In summary, the gas chromatography values did not notably contribute to errors in modeling the BPP. Although the comparison of the C_7+ fraction in the vapor phase to the C_7+ fraction in liquid phase is not rigorous due the differences in their molecular weights, no significant error was introduced by this assumption. Almost all of the error was contributed from the measurement of the G/L ratio and the experimental measurement of the BPP. The error in the G/L ratio impacted the model results for the BPP. At BPPs less than 20 psig, the error associated with the modeled BPP was significantly less that the experimentally measured BPP.

VII. Conclusions and Recommendations

In order to analyze samples in the future for possible air infiltration, the oxygen concentration of the flash sample phases should be measured. The nitrogen resulting from added air could then be distinguished from the nitrogen in the stored cavern crude oil. While the BPP could not be accurately measured with any added nitrogen, a credible BPP could be calculated.

The concentration of the light ends in the flash liquid fraction is too low. This error manifests itself in lower calculated BPPs. Use of the vapor phase concentrations and equilibrium constants to predict the liquid composition was found to be a reasonable approximation, and introduced less error, than to directly use the liquid fraction compositional data. The SPR samples have a very low gas:liquid flash ratio. Thus, a small error in the liquid fraction light ends will have a significant error in the calculated cavern composition. Unless additional care is taken in preserving the integrity of the liquid flash samples, use of the gas flash fraction analysis to predict the liquid flash fraction composition is recommended.

The samples taken at the Big Hill site have an associated error(s) that cannot be attributed to sampling scheme, date, or sample cylinder type. To a first order, there is no significant variation among the three other major sites in terms of sampling scheme, date, or sample cylinder type.

The gas chromatography analysis of the gas samples did not contribute a significant error in modeling the BPP. Although the comparison of the C_7+ fraction in the vapor phase to the C_7+ fraction in liquid phase is not rigorous due the differences in their molecular weights, no significant error was introduced by this assumption. Error was introduced in the measurement of the G/L ratio and the BPP. Therefore, a stochastic technique similar to the method outlined in section VI is recommended in future analyses in order to minimize the impact of errors and gain a higher level of confidence in the measurement of the BPP.

VIII. References

[1] T.E. Hinkebein, et. al, "Gas Intrusion into SPR Caverns," SAND 95-0023 (1995).
[2] R.C. Reid, J.M. Prausnitz, B.E. Poling, "The Properties of Gasses and Liquids," 4th ed., McGraw-Hill, (1987).
[3] H. Knapp, "Vapor-Liquid Equilibria for Mixtures of Low Boiling Substances," DECHEMA, vol. VI (1982).
[4] C.J. King, "Separation Processes," 2nd ed., McGraw-Hill, pp64-80 (1980).
[5] F.B. Hildebrand, "Advanced Calculus for Applications," Prentice-Hall, pp352-359 (1962).

Table 1. Nomenclature	
A. B	cubic equation parameter of mixture
a_i, a_j, b_i	parameter of the ith or jth component
a_m, b_m	parameter of mixture
BPP	bubble point pressure
$BPP_{experiment}$	experimentally measured bubble point pressure
BPP_{model}	modeled bubble point pressure
E_i	variance of variable i
F	optimization function
f_w	function of acentric factor
H_i	Henry's Law constant for component i
K_i	equilibrium constant for component i
k_{ij}	interaction narameter between component i and i
L	optimization function
L/F	molar ratio of flash liquid product to total molar feed
M_1, M_2	balances for statistical adjustment
n	number of variables in statistical adjustment routine
P	absolute pressure of mixture
P_c	critical pressure of component
R	universal gas constant
S_i	original value of variable i
S_i^*	adjusted value of variable i
T	temperature of mixture
T_c	critical temperature of component
T_r	reduced temperature of component
w	acentric factor
x_i, x_j	liquid mole fraction of component i or j
y_i, y_j	vapor mole fraction of component i or j
Z	compressibility factor
z_i, z_j	overall (cavern) mole fraction of component i or j
α	approach narameter used in equation 2 1
δ_i	combined narameter used in equations 12 & 13
λ_1, λ_2	eigen values of balances M_1 and M_2
φ_{1i}, φ_{2i}	partial derivative of balances M_1 and M_2 with S_i
ϕ_i	fugacity coefficient of component i

Table 2. Agreement of Site Modeled and Experimental Bubble Points						
		Site Sample Distribution				
Site	Overall Agreement	Down Hole	Surface	Coiled Tubing	Skid	Weighted Average
Bayou Choctaw	18%	52%	36%	0%	12%	17%
Big Hill	6%	31%	37%	6%	25%	23%
Bryan Mound	21%	41%	34%	11%	14%	22%
West Hackberry	22%	49%	36%	2%	4%	18%
Overall Agreement		12%	18%	55%	35%	

Table 3. Summary of Site Sample Schedule					
Dates of Sampling	Bayou Choctaw	Big Hill	Bryan Mound	West Hackberry	Average of All Sites
10/91-1/93 4/95-7/95	8%	29%	16%	20%	18%
4/93-1/95	92%	71%	84%	80%	82%

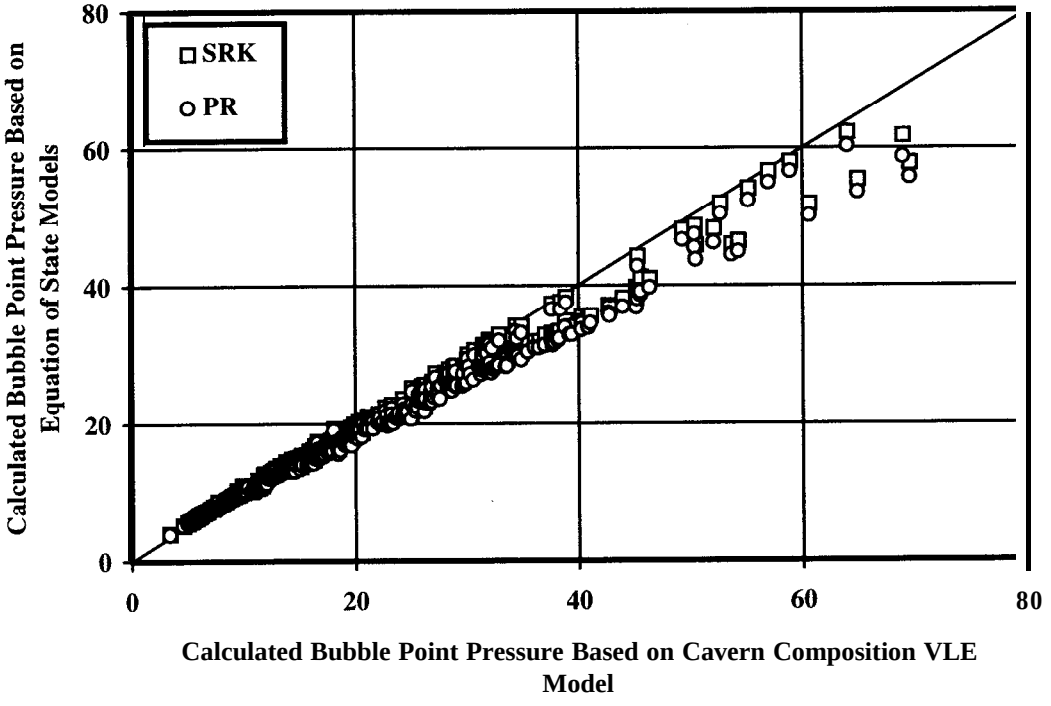

Figure 1. Comparison of Model Bubble Point Pressure Techniques

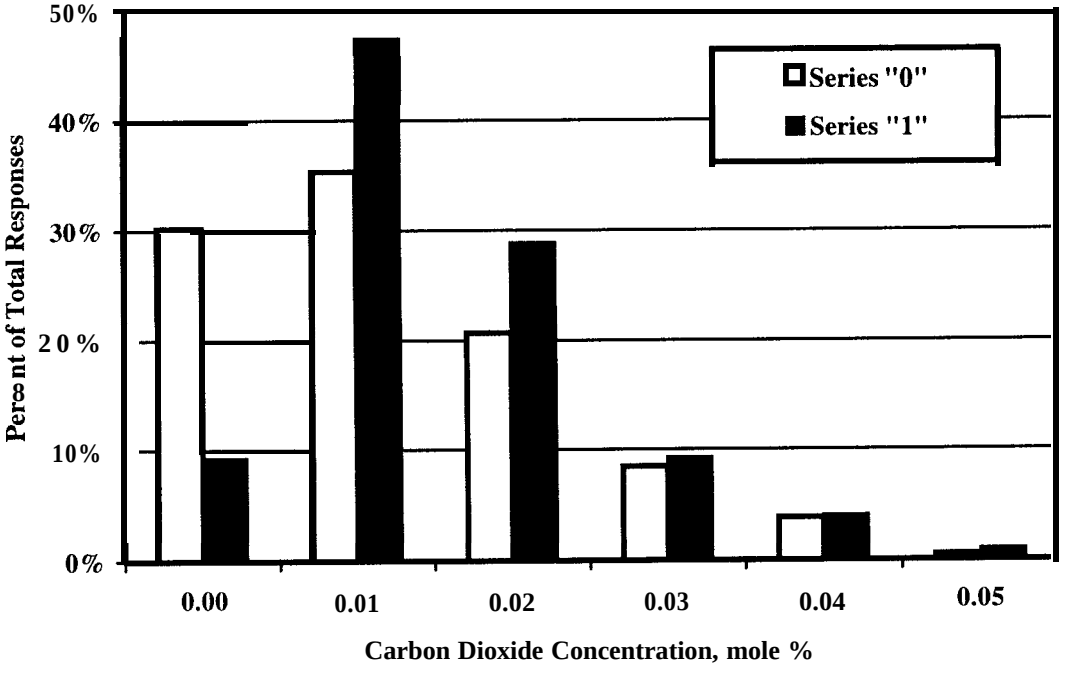

Figure 2. Effect of CO_2 on Correlation Between Experimental and Modeled BPP

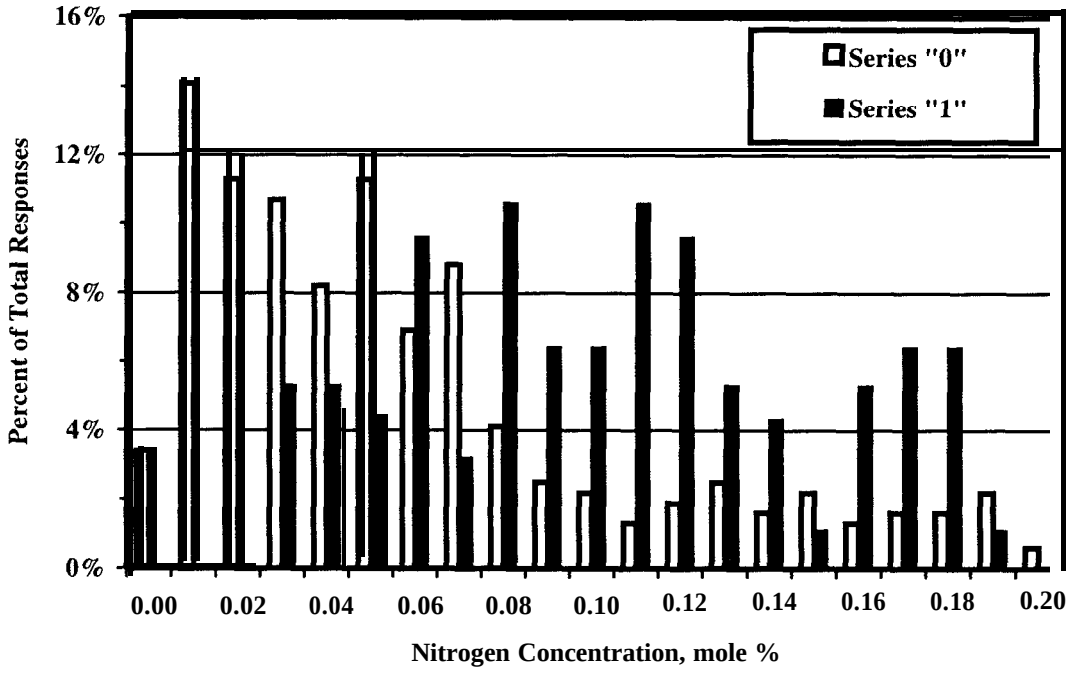

Figure 3. Effect of N_2 on Correlation Between Experimental and Modeled BPP

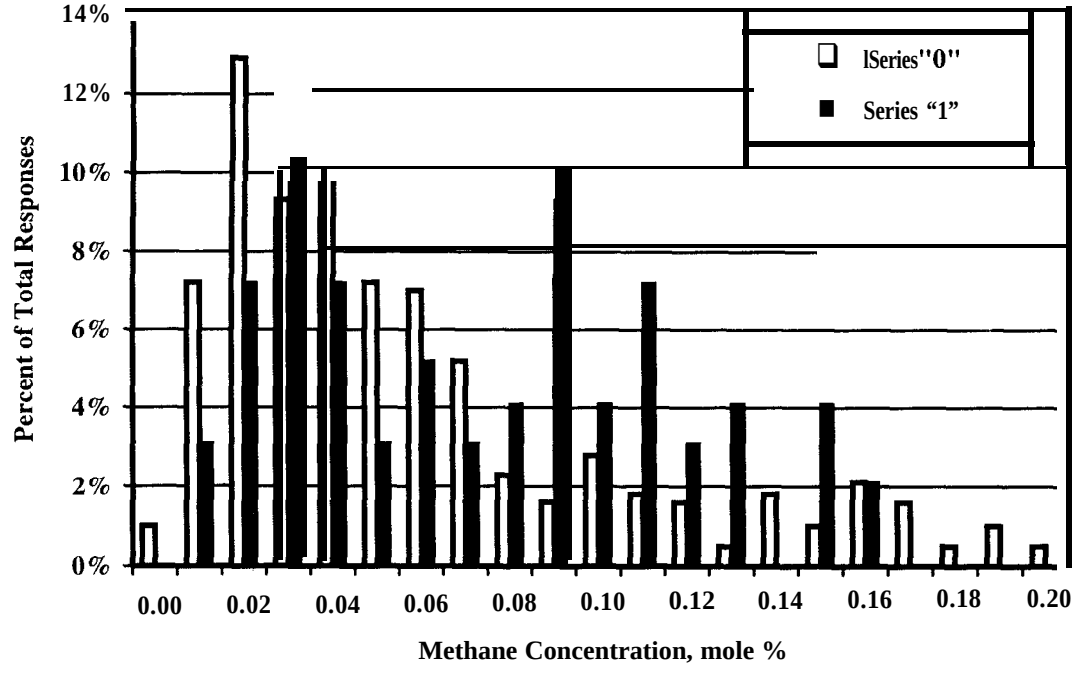

Figure 4. Effect of CH_4 on Correlation Between Experimental and Modeled BPP

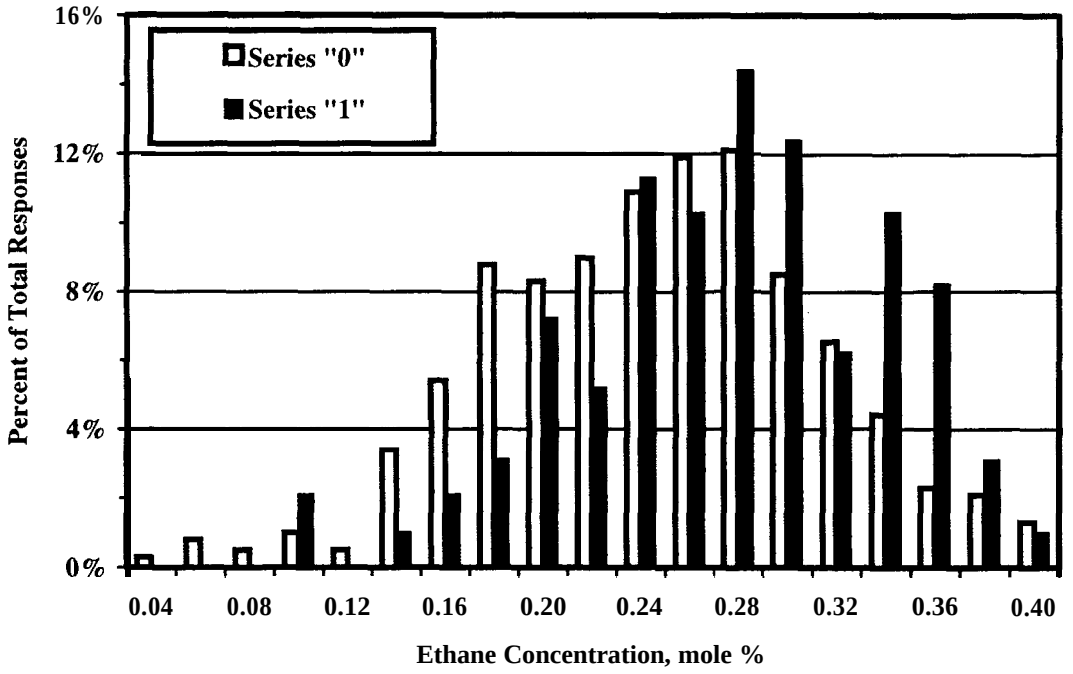

Figure 5. Effect of C_2H_6 on Correlation Between Experimental and Modeled BPP

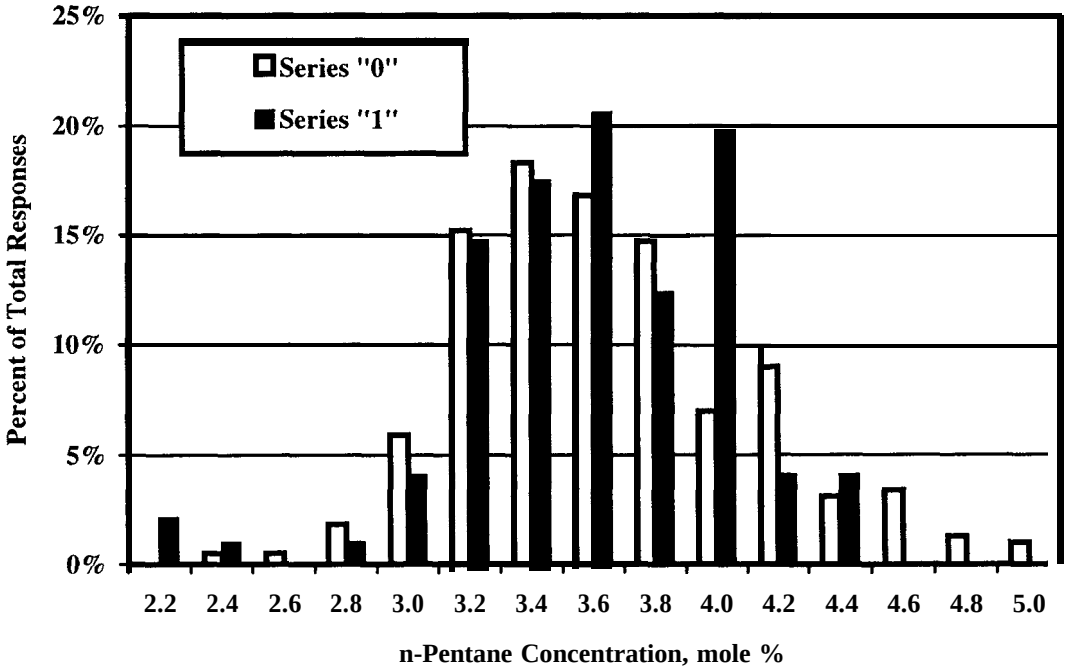

Figure 6. Effect of $n\text{-}C_5H_{12}$ on Correlation Between Experimental and Modeled BPP

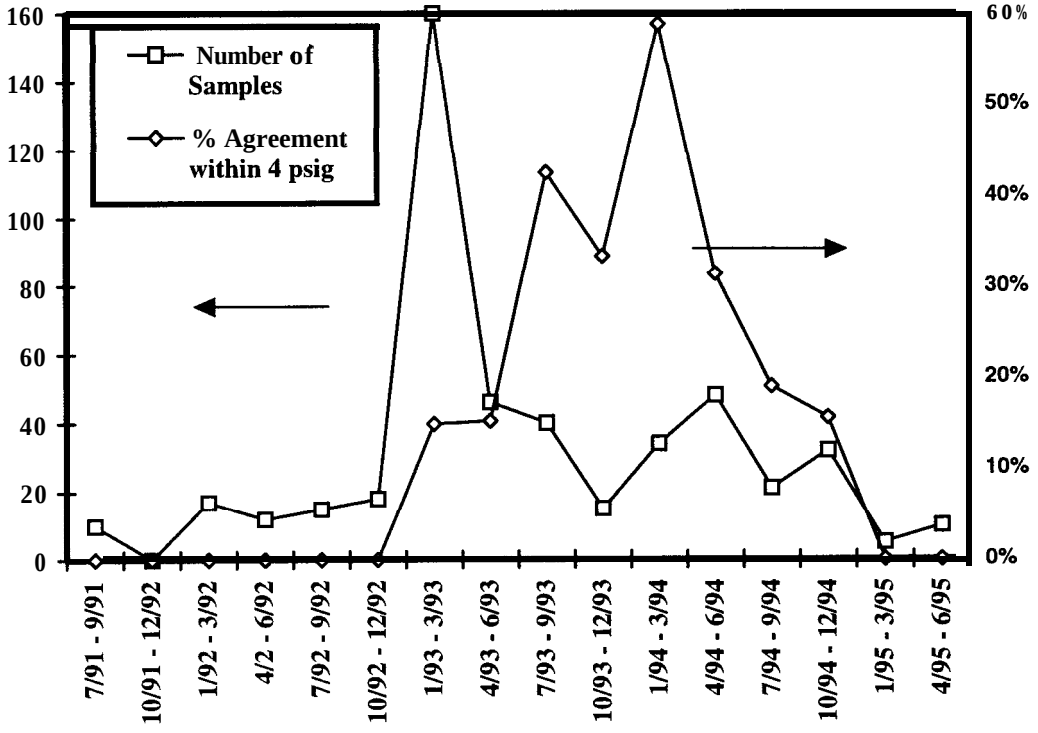

Figure 7. Sampling Dates and Agreement between Model and Experimental BPP

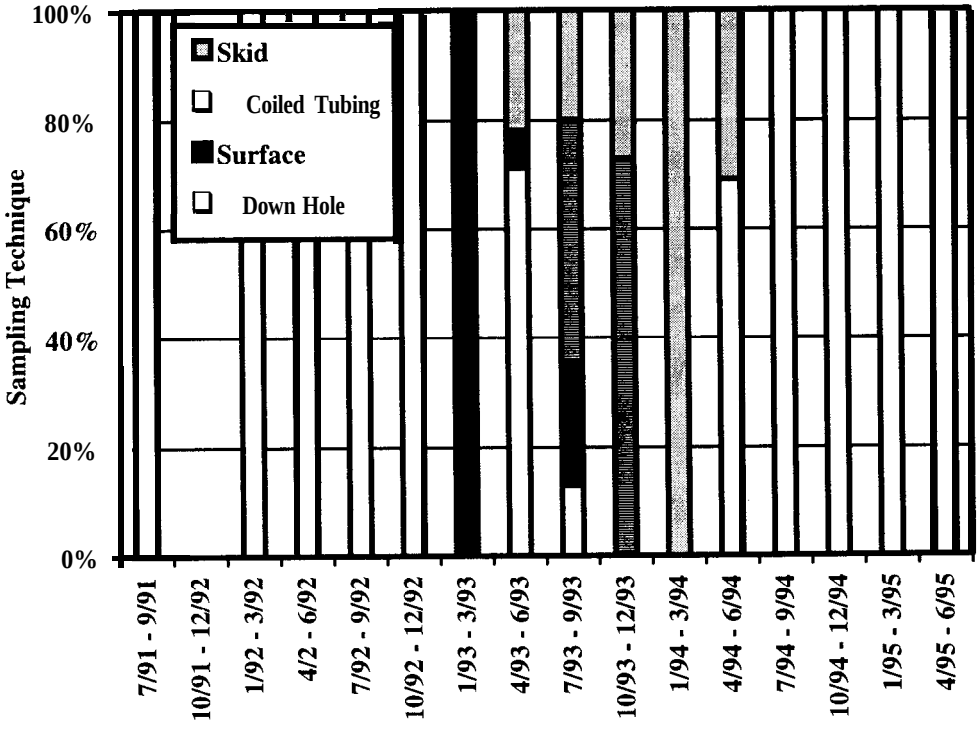

Figure 8. Histogram of Sampling Method

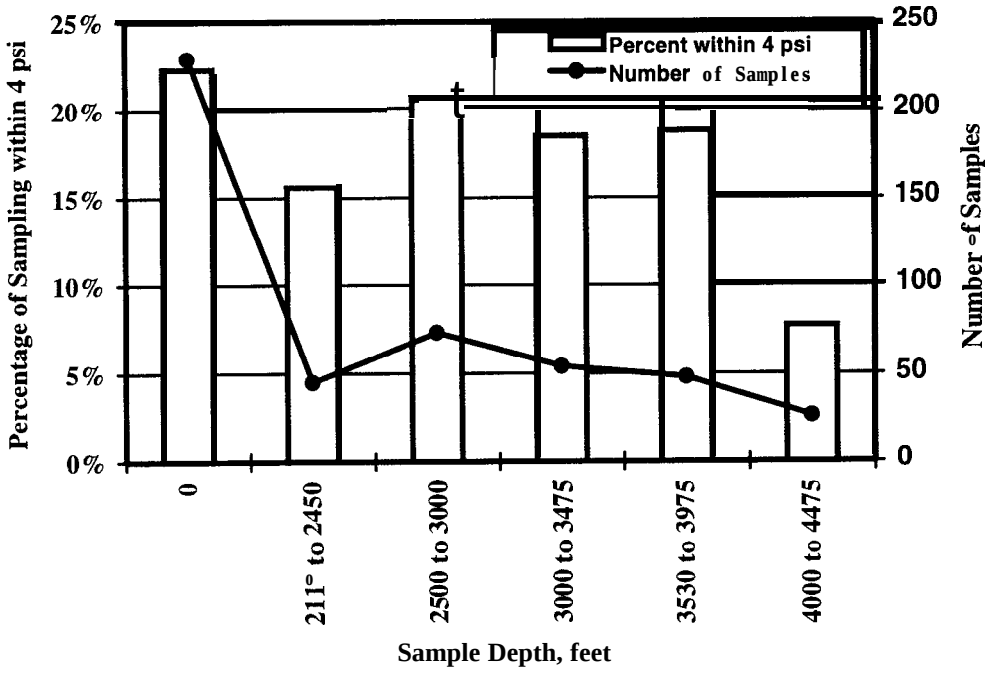

Figure 9. Agreement Between Model and Experimental BPP as a Function of Sample Depth

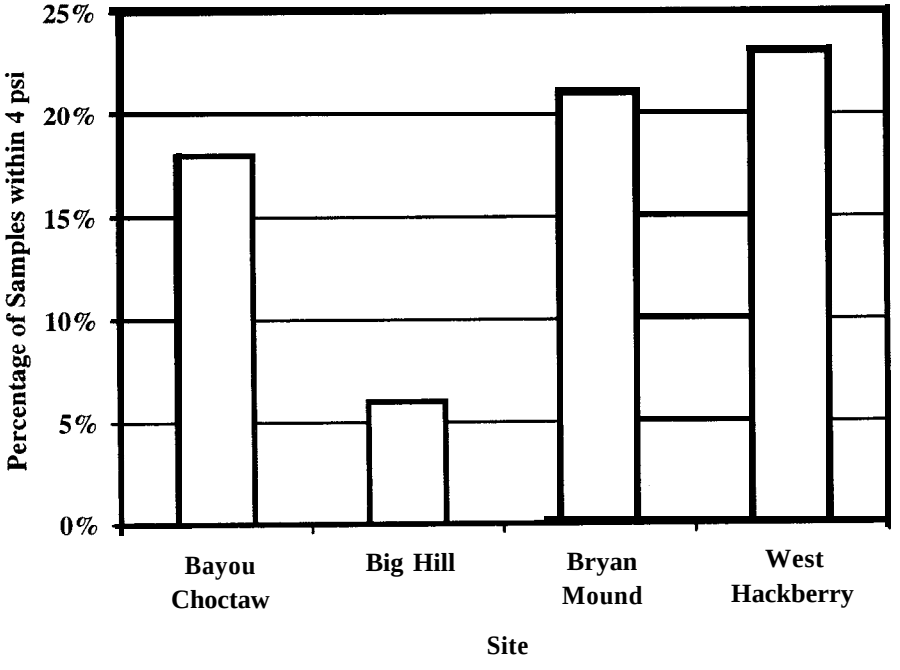

Figure 10. Agreement Between Model and Experimental BPP as a Function of Site

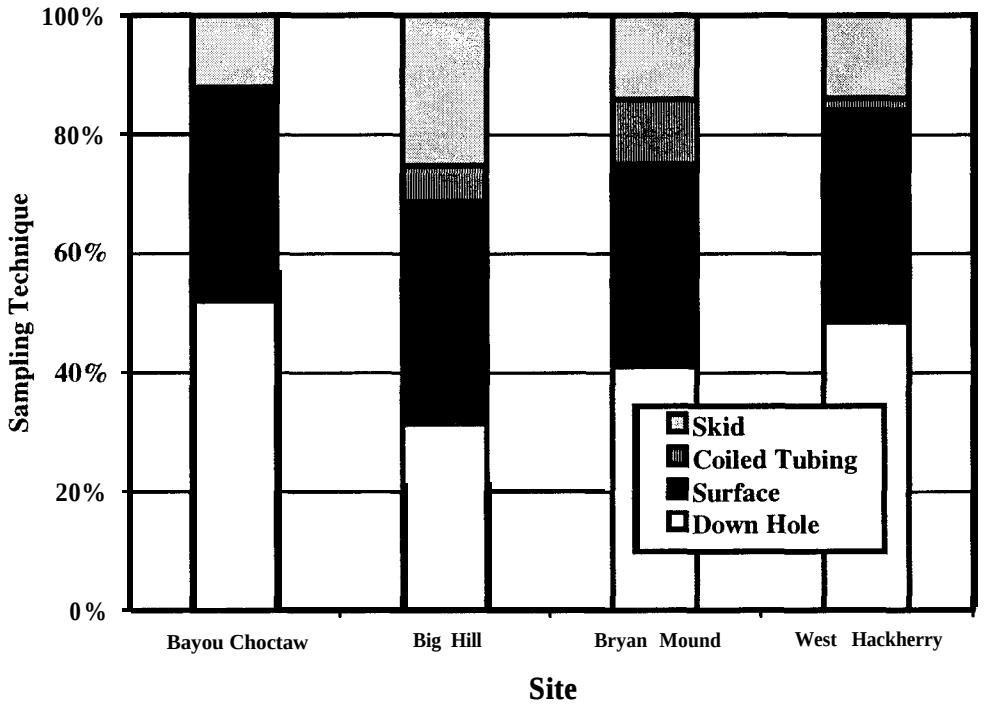

Figure 11. Sampling Scheme as a Function of Site

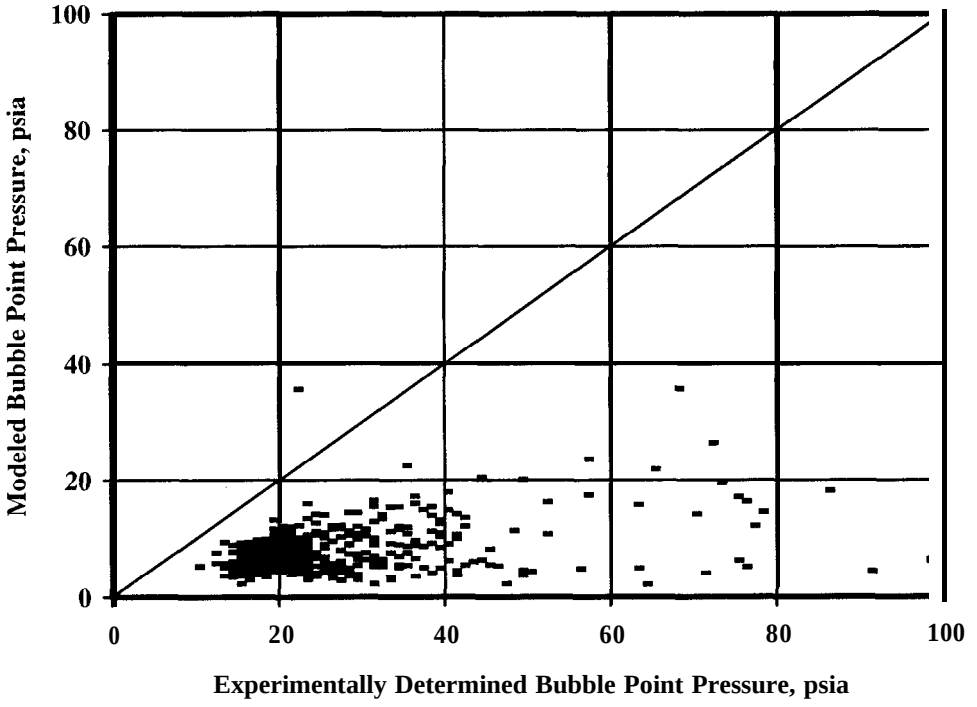

Figure 12. Vapor-Equilibrium Model Based on Liquid Compositions

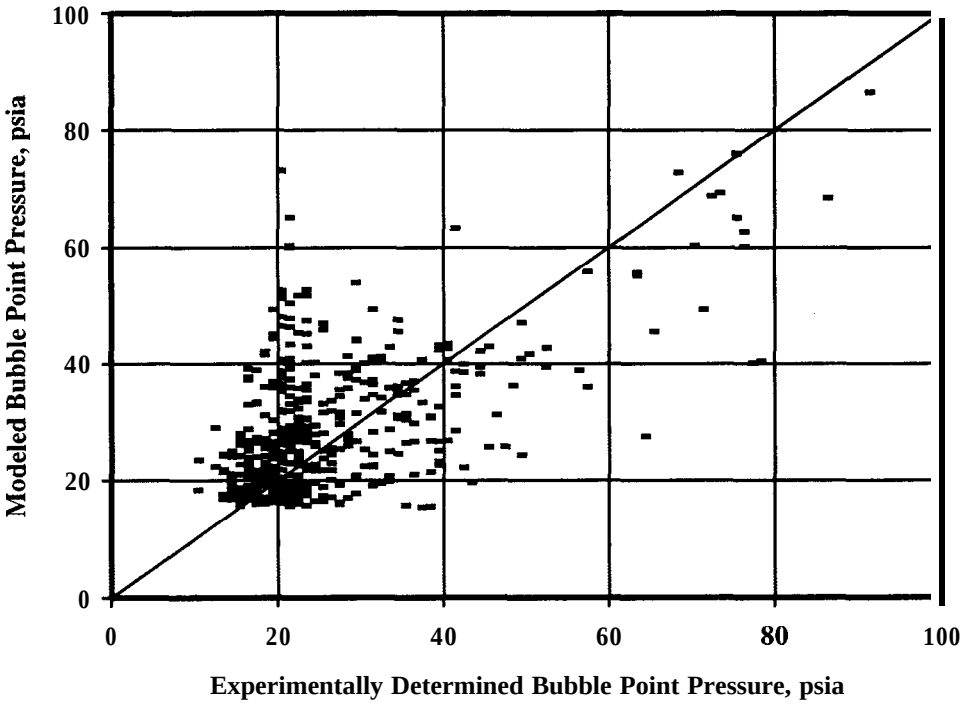

Figure 13. Vapor-Equilibrium Model Based on Vapor Compositions

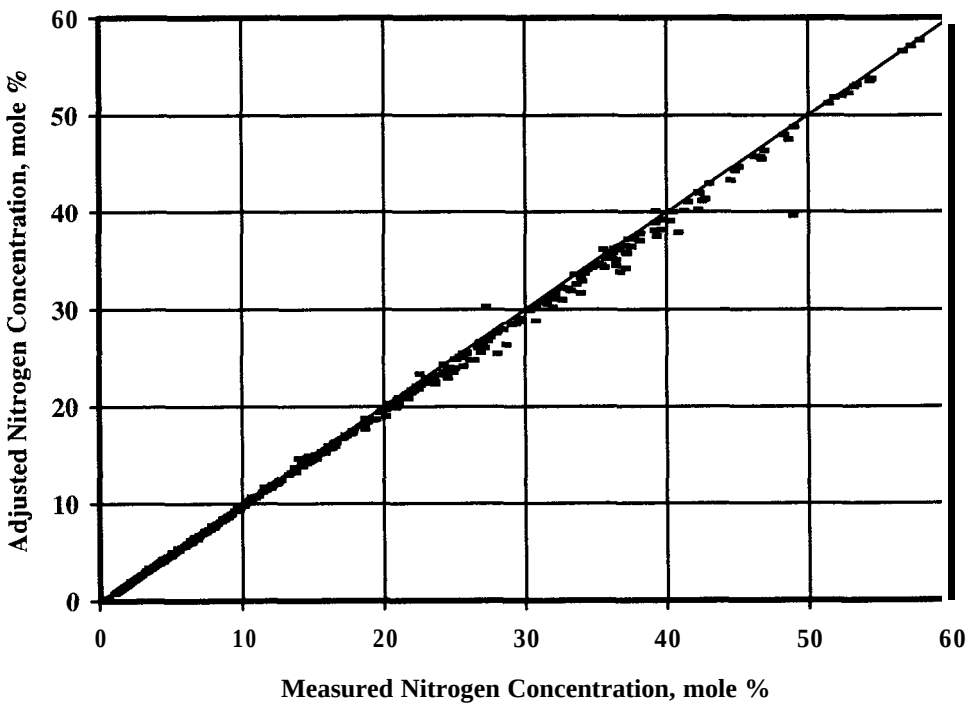

Figure 14. Adjusted Nitrogen Concentration versus Measured Nitrogen Concentration

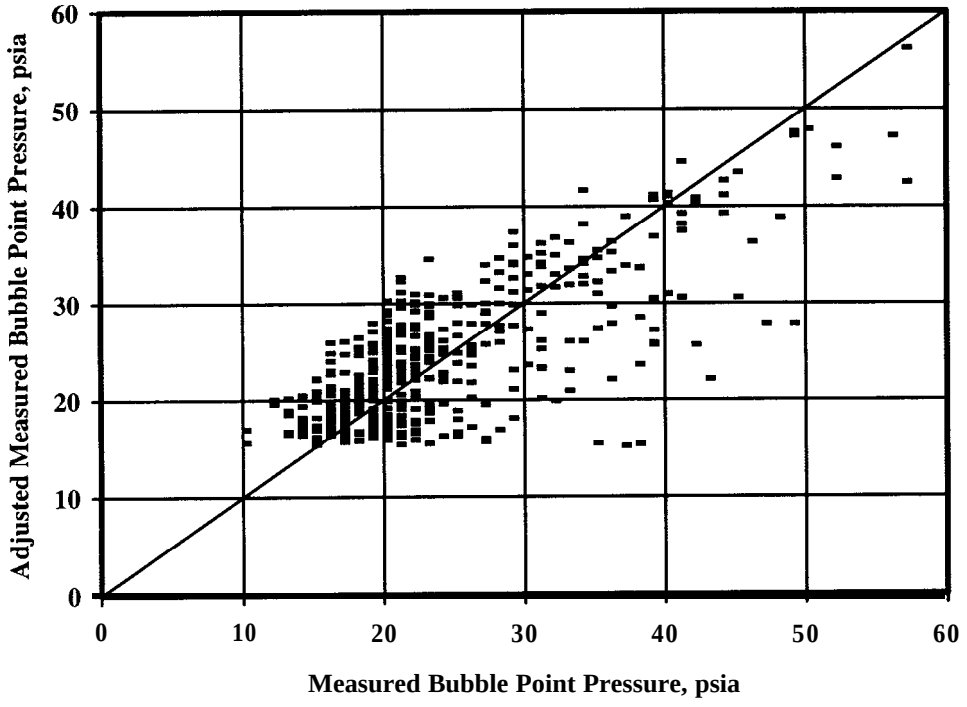

Figure 15. Adjusted Bubble Point Pressure versus Measured Bubble Point Pressure

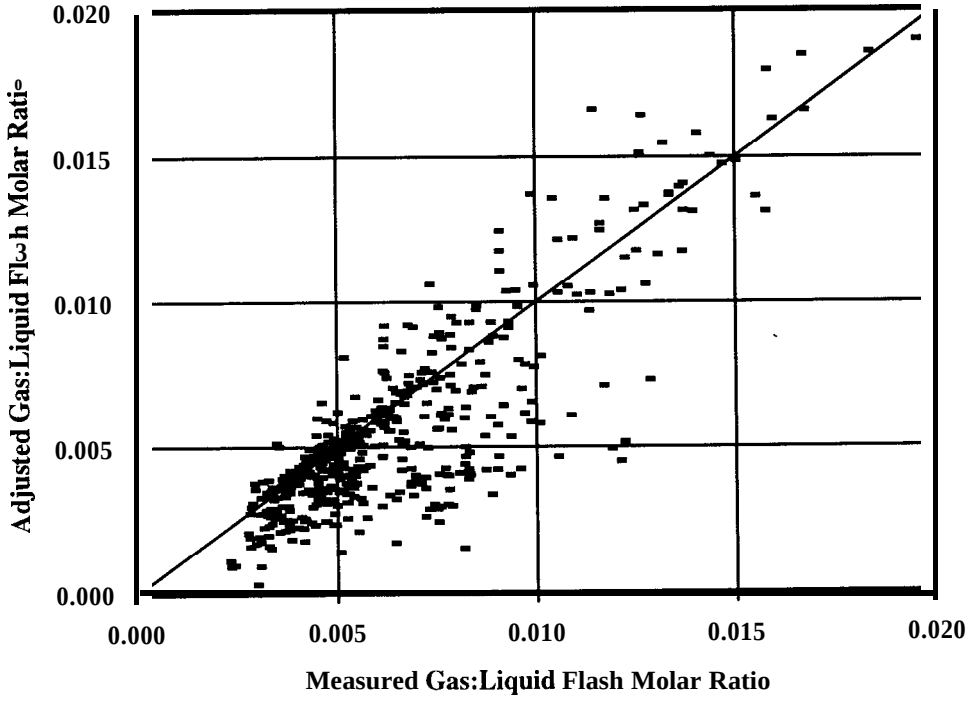

Figure 16. Adjusted G/L Ratio versus Measured G/L Ratio

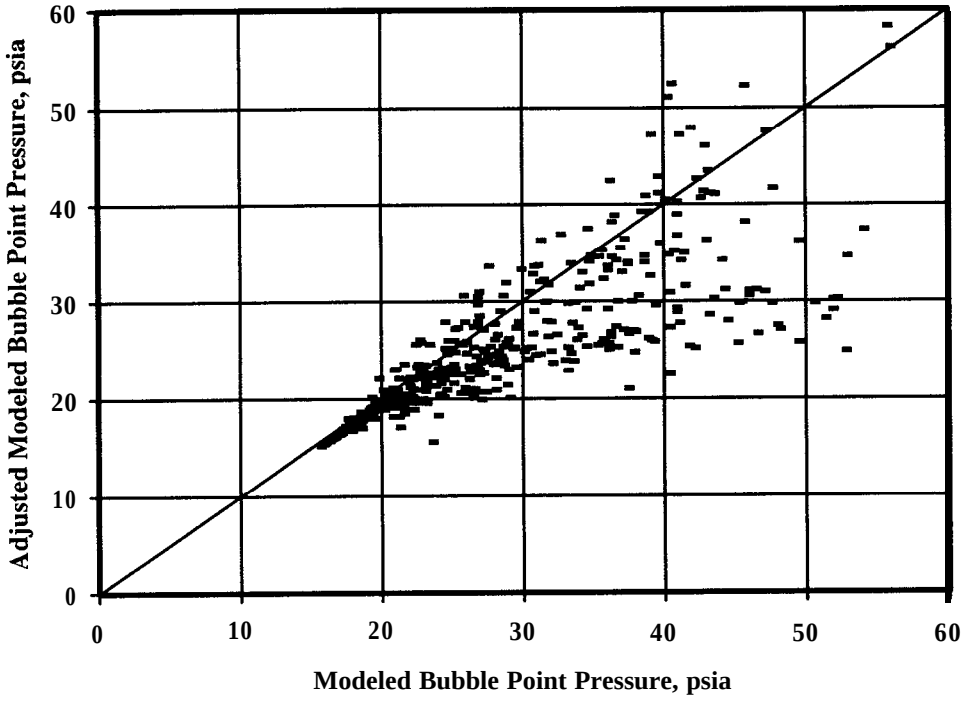

Figure 17. Adjusted Bubble Point Pressure versus Modeled Bubble Point Pressure

Distribution:

U.S. DOE SPR PMO (10)
900 Commerce Road East
New Orleans, LA 70123
Attn:
G.B. Berndsen, FE 443-l (3)
L.A. Boston, FE 4432
J. Culbert, FE 443 1
J.C. Kilroy, FE 443
J. W. Kunkel, FE 4422.1
R. E. Myers, FE 4422
TDCS (2)

Tucker & Associates, Inc.
800 Commerce Road West
Suite 500
New Orleans, LA 70123
Attn: C. Sherman

U.S. Department of Energy (4)
Strategic Petroleum Reserve
1000 Independence Avenue SW
Washington, D.C. 20585
Attn:
D. Johnson, FE 421
H.N. Giles, FE 423 (3)

DynMcDermott (3)
850 South Clearview Parkway
New Orleans, LA 70 123
Attn:
L.L. Eldredge, EF 20
G.K. Hughes, EF 32
J.H. Roche, EF 22

Bayou Choctaw SPR Site
60825 Hwy. 1148
Plaquemine, LA 70764
Attn: J.C. Morris

Big Hill SPR Site
P.O. Box 1270
Winnie, TX
Atttn: A. Fruge

West Hackberry SPR Site
1450 Black Lake Road
Hackberry, LA 70645
Attn: R. Francoeur

Sandia Internal:

MS 0701 R. W. Lynch, 6100
MS 0706 J. K. Linn, 6113 (10)
MS 0706 T.E. Hinkebein, 6113
MS 0706 S.E. Lott, 6113 (15)
MS 9018 Central Tech. Files, 8523-2
MS 0899 Technical Library, 4414 (5)
MS 0619 Print Media, 12615
MS 0100 Document Processi ng (2)
for DOE/OSTI, 76 13-2